OMAE2018–78560

SURFACE WAVES GENERATED BY A TRANSLATING AND OSCILLATING SOURCE ATOP REALISTIC SHEAR FLOWS

Yan Li [*a], **Simen Å Ellingsen**[a]
[a]Department of Energy and process Engineering
Norwegian University of Science and Technology
Trondheim, 7491
Norway
Email:yan.li@ntnu.no

ABSTRACT

We analyze surface waves generated by a translating, oscillating surface disturbance atop a horizontal background flow of arbitrary depth dependence, with a focus on determining the Doppler resonance. For a critical value of the dimensionless frequency $\tau = \omega V/g$ (ω: oscillation frequency, V: source velocity, g: gravitational acceleration) at which generated waves cannot escape. In the absence of shear the resonant value is famously $1/4$; the presence of a shear current modifies this. We derive the theoretical and numerical tools for studying this problem, and present the first calculation of the Doppler resonance for a source atop a real, measured shear current to our knowledge. Studying graphical solutions to the (numerically obtained) dispersion relation allows derivation of criteria determining the number of far-field waves that exist in different sectors of propagation directions, from which the criteria for Doppler resonance follow. As example flows we study a typical wind-driven current, and a current measured in the Columbia River estuary. We show that modeling these currents as uniform or with a linear depth dependence based on surface measures may lead to large discrepancies, in particular for long and moderate wavelengths.

1 INTRODUCTION

The studies of the fundamental problem of water waves generated by a translating, oscillating wave-maker dates back at least to the middle of the last century. The problem is central for s-tudying wave–body interactions in the frequency domain, e.g. sea-keeping performance of ships, and motions of offshore floating structures in regular waves.

A large body of literature in this regard exists in the absence of a shear current, c.f .e.g. [1–3]. In particular, a well-known phenomenon associated with the problem is Doppler resonance that is of significant physics as well as of mathematical interest. Physically, Doppler resonance occurs when the energy is held stationary in space [3, 4], which leads to a marked increase of the wave amplitude [5, 6]. Doppler resonance occurs when the nondimensional frequency $\tau = \omega V/g$ (ω and V are the oscillating frequency and moving speed of a wavemaker, respectively; g is the gravitational acceleration) reaches a resonant value $\tau_{\rm res}$. When no shear is present the resonant value is $\tau_{\rm res} = 1/4$ in deep water [3] and decreases with the depth dependent Froude number ${\rm Fr}_h = V/\sqrt{(gh)}$ (h is the water depth) [7, 8]. Wave resistance may also be noticeably increased in the vicinity of the critical value $\tau_{\rm res}$ [9,10], the resonant value poses numerical challenges [11, 12].

Studies of wave–body systems when a shear current is present are, however, scarce. It has been shown the presence of a shear current can strongly affect surface gravity waves from, and associated forces on, wave sources ("ships") in steady motion [8, 13–16]. Li & Ellingsen (2016) [17] have studied this topic when a shear current of uniform vorticity S is present. In particular, multiple resonant values $\tau_{\rm res}$ – as many as four – may occur, depending on the shear Froude number ${\rm Fr}_s = VS/g$ and the angle β between the background shear current and motion of a

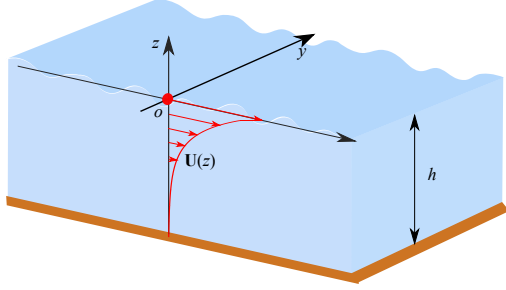*[*]Address all correspondence to this author.

FIGURE 1. Geometry of the wave-current system: gravity surface waves on an arbitrary shear current.

wavemaker. That the presence of a shear current may profoundly affect τ_{res} is further confirmed by Smeltzer et al. (2017) [8] in where the presence of a surface shear layer such as may be created by wind is considered, modeled as a bilinear profile.

Realistic currents generally vary with water depth in a more complicated fashion than either a linear or bilinear profile [18, 19]. It is thus of practical significance to allow current varying arbitrarily with water depth. The present work analyzes effects of the presence of an arbitrary depth dependent flow on properties of waves generated by a translating, oscillating wavemaker. Based on [20, 21], a direct integration method is used to numerically obtain the dispersion relation of waves. In particular, similar discussions as [17] with respect to dispersion relation of different waves are presented for this far more general case. As examples we analyze Doppler resonance in the presence of a typical wind induced shear current and a realistic current measured at the mouth of Columbia River. Specifically, the corresponding numerical results show the resonant values τ_{res} may differ significantly in the presence a realistic (nonlinear) shear current from a linear shear current of the same surface vorticity.

2 SYSTEM DESCRIPTION AND FORMALISM

Linear gravity surface waves generated by a moving, oscillating surface disturbance are considered atop a background shear flow that is expressed $\mathbf{U}(z) = (U_x(z), U_y(z))$. We consider incompressible and inviscid flow and neglect surface tension. The geometry of the system is depicted in Fig. 1. The still water surface is located at $z = 0$ and the positive z axis points upwards. The water depth h is uniform.

Due to superposition no generality is lost by expressing a surface disturbance in the form

$$\hat{\eta}(\mathbf{x}, t) = \eta_0(\mathbf{k}) \exp(\mathbf{k} \cdot \mathbf{x} - \omega(\mathbf{k})t), \tag{1}$$

in which $\hat{\eta}$ may denote motions along different directions, e.g. heave, surge and sway, or an external oscillatory pressure that is considered in the present work; $\eta_0(\mathbf{k})$ is the am-

plitudes of the corresponding motions or the pressure strength, $\mathbf{k} = k(\cos\theta, \sin\theta)$ $(k = |\mathbf{k}|)$ denotes the wave vector with θ being the direction of wave propagation, $\mathbf{x} = (x, y)$ is the position vector in the horizontal plane, ω is the oscillating frequency, and t is the time.

For further reference and convenience, we define

$$\mathbf{U}_0 = \mathbf{U}(0) = U_0(\cos\beta, \sin\beta),$$
$$\hat{w}(\mathbf{x}, z, t) = A(\mathbf{k}, z)\exp(\mathbf{k} \cdot \mathbf{x} - \omega(\mathbf{k})t),$$
$$\sigma(\mathbf{k}) = \omega - \mathbf{k} \cdot \mathbf{U}_0, \ \Delta\mathbf{U}(z) = \mathbf{U}(z) - \mathbf{U}_0,$$

in which U_0 is the magnitude of the surface velocity, β is the angle between the surface velocity $\mathbf{U}_0$ of a shear current and x axis, $\hat{w}$ is the vertical velocity due to waves, whose amplitude is $A(\mathbf{k}, z)$, and σ is the intrinsic frequency.

2.1 Dispersion relation

In order to seek solutions of the perturbations generated by the surface disturbance expressed by (1), we may refer to a couple of recent papers that analyze waves in the presence of a depth dependent, horizontal background current, e.g. [15, 17]. In particular, a generalized theory of linear waves atop a background shear flow can be found in [20]. We follow the theory presented in [20, 21]. The linearized governing equation and boundary conditions for our set-up are well known (e.g. [22])

$$\bar{w}''(\mathbf{k}, z) - k^2 \bar{w}(\mathbf{k}, z) = \frac{\mathbf{k} \cdot \mathbf{U}''(z)}{\omega - \mathbf{k} \cdot \mathbf{U}(z)} \bar{w}(\mathbf{k}, z), \ z < 0, \tag{2a}$$

$$\bar{w}(\mathbf{k}, z) = 1, \ \text{at } z = 0, \tag{2b}$$

$$\bar{w}(\mathbf{k}, z) = 0, \ \text{at } z = -h, \tag{2c}$$

in which $\bar{w} = A(\mathbf{k}, z)/A(\mathbf{k}, 0)$ is called the unity vertical velocity and the prime denotes the derivative with respect to z. (2a) is obtained from the linearized continuity and Euler equation and is called the Rayleigh equation.

The linearized kinematic and dynamic boundary conditions at the water surface yield

$$\sigma^2 \bar{w}' - \mathbf{k} \cdot \mathbf{U}_0' \sigma - gk^2 = 0, \ \text{at } z = 0, \tag{3}$$

in which $\bar{w}(\mathbf{k}, 0) = 1$ is applied.

Based on (2a) and (3), we may find the dispersion relation whose detailed derivation can be found in [15]. It reads

$$\Delta_R(\mathbf{k}, \omega(\mathbf{k})) \equiv \sigma^2 + I_{\text{cur}}\sigma - gk\tanh kh = 0, \tag{4}$$

2

in which

$$I_{\mathrm{cur}} = (I_S + I_N)\tanh kh, \qquad (5a)$$

$$I_S = \frac{\mathbf{k}\cdot\mathbf{U}_0'}{k}, \qquad (5b)$$

$$I_N = \int_{-h}^{0} \frac{\sigma\mathbf{k}\cdot\mathbf{U}''(z)\bar{w}(\mathbf{k},z)\sinh k(z+h)}{(\sigma - \mathbf{k}\cdot\Delta\mathbf{U}(z))k\sinh kh}\mathrm{d}z, \qquad (5c)$$

where I_S is called the surface shear and I_N the depth-averaged shear. When the latter is equal to zero, it denotes the presence of a shear current of uniform vorticity. In addition, a critical layer may occur when $\sigma = \mathbf{k}\cdot\Delta\mathbf{U}$ that makes I_N improperly defined and thus special care is needed [22, 23]. We will not focus on this particular case herein, but it is straightforward to extend the results from the present paper to cases where a critical layer exists, i.e. we take the principle value of I_N rather than I_N when a pole appears in the integrand.

Note that both $\mathbf{k}$ and $\bar{w}$ in (4) are unknown at a given $\omega = \omega_0$, which makes (4) non-closed. Nevertheless, the coupled problem consisting of (2) and (4) can be solved with respect to unknowns $\mathbf{k}$ and $\bar{w}(z)$ by numerical methods, e.g. a shooting method introduced in Dong & Kirby (2012) [24] or a direct integration method studied in [20, 21]. We use the latter that essentially solves (2) and (4) by an iterative approach. This method calculates $\bar{w}(z)$ and σ for a chosen set of discrete values of z varying from $-h$ to 0.

Based on (4), we obtain

$$\omega(\mathbf{k}) - \mathbf{k}\cdot\mathbf{U}_0 = \sigma_{\pm}$$
$$\equiv \pm\left(\sqrt{gk\tanh kh + \frac{1}{4}I_{\mathrm{cur}}^2} \mp \frac{1}{2}I_{\mathrm{cur}}\right), \qquad (6)$$

which implies

$$\omega(\mathbf{k}) = -\omega(-\mathbf{k}), \qquad (7)$$

meaning that there is a unique and positive phase velocity ω/k pertaining to each wave vector $\mathbf{k}$.

According to (4) and (6), we know that contributions from a shear current are included in the current relevant term I_{cur} that returns zero when there is no shear current. We write

$$I_{\mathrm{cur}} = \int_{-h}^{0}\left(1 + \frac{\sigma}{\sigma - \mathbf{k}\cdot\Delta\mathbf{U}}\frac{\bar{w}\sinh k(z+h)}{\sinh kh}\right)$$
$$\times \frac{\mathbf{k}\cdot\mathbf{U}''(z)}{k}\mathrm{d}z \qquad (8)$$

in which the inequality $\bar{w}\sinh k(z+h)/\sinh kh \leq 1$ holds for $z \in (-h, 0)$. We in addition assume $|\varepsilon| = \left|\dfrac{\mathbf{k}\cdot\Delta\mathbf{U}}{\sigma}\right| < 1$ and then obtain

$$I_{\mathrm{cur}} = \int_{-h}^{0}(1+N)\frac{\mathbf{k}\cdot\mathbf{U}''(z)}{k}\mathrm{d}z \qquad (9)$$

$$N = \frac{\bar{w}\sinh k(z+h)}{\sinh kh}\sum_{j=0}^{\infty}\varepsilon^{j}, \qquad (10)$$

in which N denotes the depth-dependent shear contributions relative to the surface vorticity of an arbitrary depth dependent current. Eq. (9) compares the influence on dispersion of the surface vorticity and the depth–averaged shear, respectively. For different range of ε values, different approximate dispersion relations can be obtained, as studied in [23].

In deep water, we may readily obtain the dispersion relation by taking the limit $kh \to \infty$

$$\Delta_{R_{inf}}(\mathbf{k},\omega(\mathbf{k})) \equiv \sigma^2 + I_{\mathrm{cur}_{inf}}\sigma - gk = 0, \qquad (11)$$

$$I_{\mathrm{cur}_{inf}} = \frac{\mathbf{k}\cdot\mathbf{U}_0'}{k} + \int_{-\infty}^{0}\frac{\mathbf{k}\cdot\mathbf{U}''\sigma\bar{w}}{k(\sigma - \mathbf{k}\cdot\Delta\mathbf{U})}\mathrm{e}^{kz}\mathrm{d}z. \qquad (12)$$

Eq. (6) can be expressed with graphical solutions, as will be demonstrated in §2.3. It is readily verified that the inequality $\sqrt{gk\tanh kh + I_{\mathrm{cur}}^2} - I_{\mathrm{cur}} \geq 0$ holds for all $\mathbf{k}$. Before seeking the graphical solutions of (6), we introduce the nondimensional parameters that are defined

$$K = kh;\ \mathrm{Fr}_h = \frac{U_0}{\sqrt{gh}};\ \mathrm{Fr}_s = \frac{U_0 S}{g};\ \mathrm{Fr}_{sb} = S\sqrt{\frac{h}{g}};$$

$$\Omega = \omega\sqrt{\frac{h}{g}};\ \tau = \frac{\omega U_0}{g} = \mathrm{Fr}_h\Omega;\ \Sigma_{\pm} = \sigma_{\pm}\sqrt{\frac{h}{g}},$$

in which the water depth h is used as the reference length, $S = |\mathbf{S}|$ (where $\mathbf{S} = \mathbf{U}'(0) = (U_x'(0), 0)$, i.e. we always define the $\mathbf{S}$ along the positive x axis) is the surface vorticity of the shear current, and Fr_s and Fr_{sb} are the surface shear Froude numbers that are defined based on the reference length $\sqrt{g/S^2}$ and $\sqrt{gh}$,

FIGURE 2. Definition of angles. See text for details.

FIGURE 3. Graphic solutions of the dispersion relation. See text for details.

respectively. Thereby, the nondimensional expression of (6) is

$$\Omega(\mathbf{k}) + K \mathrm{Fr}_h \cos\gamma = \Sigma_\pm(K, \gamma + \beta), \tag{13}$$

$$\Sigma_\pm = \pm \left[\sqrt{K \tanh K + \left(\frac{\mathrm{Fr}_{sb} \cos(\gamma+\beta)}{2} + \frac{\mathrm{Fr}_{SN}}{2} \right)^2 \tanh^2 K} \right.$$
$$\left. \mp \left(\frac{\mathrm{Fr}_{sb} \cos(\gamma+\beta)}{2} + \frac{\mathrm{Fr}_{SN}}{2} \right) \tanh K \right],$$

in which $\gamma = \theta - \beta$ and $\mathrm{Fr}_{SN} = I_N \sqrt{\frac{h}{g}}$ is a depth–averaged shear Froude number. An illustration of the different angles involved is depicted in Fig. 2.1. Based on (13), we observe the behaviour of Σ at large K, i.e.+ $\lim_{K\to\infty} \Sigma_\pm \sim \pm\sqrt{K}$ (note that Fr_{sb} and Fr_{SN} are order unity for most naturally appearing shear currents). This is one of the important features of $\Sigma_\pm$ in order to use graphical solutions that will be introduced in §2.3.

Solutions to (13) cannot be expressed explicitly except in a very few special cases. We will discuss the different wave solutions for a given Ω_0, $K_0(\gamma)$, in §2.3 from both a mathematical and a physical perspective with graphical solutions.

2.2 Group and phase velocity

According to the definition, phase and group velocity are defined, respectively,

$$c = \frac{\Omega(K,\gamma)}{K}, \tag{14}$$

$$\mathbf{c}_g = (c_{gK}, c_{g\theta}) = \nabla_\mathbf{K}\Omega(K,\gamma), \tag{15}$$

in which $\nabla_\mathbf{K} = (\frac{\partial}{\partial K}, \frac{\partial}{K\partial\theta})$.

Based on the dispersion relation (4), we may derive the implicit expressions of the phase and group velocity, which are easily obtained at $K_0(\gamma)$ by numerical methods.

2.3 Different waves and wave sectors

Similar to the analysis made in [17], we use graphical solutions of (13) to indicate far-field wave solutions $K_0(\gamma)$ under different circumstances, whereupon analysis of the solutions that exist in different wave propagation sectors is presented. The analysis follows the principles of §3.7.1 of [25], and one may refer to [17] for the generalization to the presence of a linear shear current. The present case is a further generalization along the same lines.

Fig. 3 depicts different graphical solutions to the dispersion relation (13) at a given Ω_0, using a typical wind–driven shear current as example. Plotted as a function of K are the straight lines $\Omega_0 + K\mathrm{Fr}_h\cos\gamma$, and the curves $\Sigma_\pm(K,\gamma)$ at different propagation angles γ. Thus, the intersection points $K_0(\gamma)$ of the two are solutions to the dispersion (13). Rich physics can be found at the intersections. Let A be a point where a line and a curve cross. Then the group velocity component c_{gK} is found at A by the difference between the slope of the tangent of Σ — $\partial\Sigma/\partial K$ — and that of the straight line, $\mathrm{Fr}_h\cos\gamma$. The intrinsic phase velocity Σ/K_0 is the slope of the straight line that connects A and the origin.

When $\cos\gamma < 0$ ($|\gamma| > \pi/2$ or $\mathbf{k}\cdot\mathbf{U}_0 < 0$), two solutions for $K_0(\gamma)$ exist, denoted K_B and K_C in Fig.3. When $\cos\gamma > 0$, three different cases exist depending on the parameters Ω_0, Fr_h, γ, Fr_{sb}, and Fr_{SN}. There can be zero far–field waves (case 1: no intersec-

tion), one wave (case 2: one intersection point, F) and two waves – D and E – of different wavenumbers (case 3: two intersection points). The group velocities for these cases satisfy, respectively, $c_{gK} < 0$ for $K \geq 0$ (case 1), $c_{gK} = 0$ at K_F (case 2), and $c_{gK} > 0$ at K_D (case 3), and $c_{gK} < 0$ at K_E (case 3). A wave with positive (negative) intrinsic group velocity will be found in front (behind) of the oscillating source, hence the only wave solution able to propagate ahead of the source is D. For more details about the different far-field waves, one may refer to [26].

As is indicated in Fig. 3, for a given value of $\mathrm{Fr}_h > 0$ there exists a critical frequency Ω_c so that when $\Omega_0 > \Omega_c$ a sector of γ values exists that belongs to Case 1. For 2D systems, $\Omega_0 = \Omega_c$ always corresponds to the Doppler resonance frequency. The 3D case will be discussed in §2.4.

As noted in the above discussions, three cases exist that depend on the parameters Fr_h, Ω_0, Fr_{sb}, γ, and Fr_{SN} for $\cos\gamma > 0$. Thus, criteria are needed in order to determine different wave solutions. We introduce the function

$$\Phi(\Omega, \mathrm{Fr}_h, \mathrm{Fr}_s, \beta, K, \gamma) = \min_{K(\gamma) \geq 0} (\Delta_R) \mathrm{sgn}(\max_{K(\gamma) \geq 0} (\Delta_R)),$$
$$\gamma \in (-\pi/2, \pi/2), \qquad (16)$$

useful for determining different cases discussed above, and it permits us to write down the criteria for the different cases succinctly:

Case 1: $\Phi > 0$, indicating no waves propagate along direction γ.
Case 2: $\Phi = 0$, indicating F waves.
Case 3: $\Phi < 0$, i.e. $\min_{K \geq 0} \Delta(\Omega, \mathrm{Fr}_h, \mathrm{Fr}_s, \beta, K, \gamma) < 0$ and $\max_{K \geq 0} \Delta > 0$, implies D and E waves.

Based on the criterion of Case 1, it is straightforward to calculate the wave sector (or sectors) of angles γ wherein there is no wave. Moreover, the criterion of Case 2 plays an essential role in determining the Doppler resonance as will be explained in §2.4.

2.4 Doppler resonance

As is discussed in §2.3, $c_{gK} = 0$ in Case 2 for waves propagating along direction γ. If $c_{g\theta}$ in addition also equals zero, $|\mathbf{c}_g| = 0$, and the energy of this particular F wave can not escape, and Doppler resonance will occur. We thus obtain the criterion for resonance in the form of a set of two equations,

$$|\mathbf{c}_g| = \sqrt{\left(\frac{\partial\Omega}{\partial K}\right)^2 + \left(\frac{1}{K}\frac{\partial\Omega}{\partial\theta}\right)^2} = 0, \qquad (17a)$$
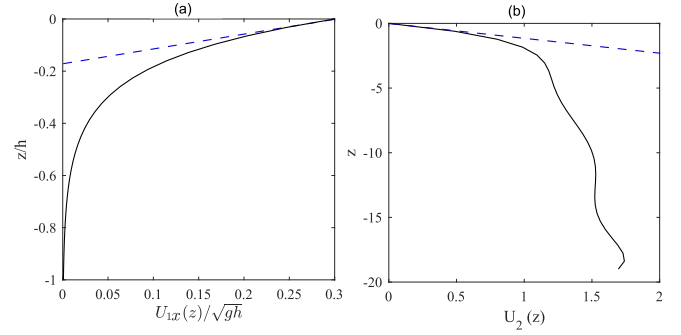$$\mathbf{c}_g = (c_{gK}, c_{g\theta}) = 0, \qquad (17b)$$

FIGURE 4. Shear Profiles: (a) the exponential shear current profile $\mathbf{U}_1$ with $\mathrm{Fr}_h = 0.3$ and $\alpha = 6$ and (b) the current $\mathbf{U}_2$ at the mouth of Columbia River. The dashed lines in the figure are the corresponding linear shear currents of the same vorticity as the corresponding shear current.

Eq. (17), together with the dispersion relation (4), yields the dimensionless resonant frequency τ_{res}. In the absence of shear it famously equals $1/4$ [3], and when a shear current is present it can take more than one value [17].

Numerically, we first find $\mathbf{K}_{\mathrm{res}} = (K_F, \gamma_{\mathrm{res}} + \beta)$ that satisfies (17) and then substitute $\mathbf{K}_{\mathrm{res}}$ to the dispersion relation (13) to obtain the Doppler resonant value $\tau = \tau_{\mathrm{res}}$. As noted above, finding $K_F(\gamma_F + \beta)$ ($\gamma \in \langle -\pi/2, \pi/2]$) is not in itself sufficient to yield τ_{res}, but $K_F(\gamma_{\mathrm{res}} + \beta)$ is important for being the wavenumber required in order to obtain τ_{res}. Any numerical solutions $\tau_{\mathrm{res}} < 0$ can be discarded as unphysical.

3 NUMERICAL RESULTS AND LIMITING CASES

In this section, we present numerical results in the presence of different shear currents. In particular, a typical wind-induced shear current $\mathbf{U}_1$ and a current $\mathbf{U}_2$ measured in the mouth of Columbia River [27] (with polynomial fit as in [15]) are considered. $\mathbf{U}_1$, plotted in Fig. 4a, is expressed

$$\mathbf{U}_1 = (U_x, U_{y0}) = (\mathrm{Fr}_h\sqrt{gh}\, e^{\alpha z/h}, U_{y0}), \qquad (18)$$

where U_{y0} is a constant, and $\mathbf{U}_2$ is plotted in Fig. 4b. We compare results in the presence of either $\mathbf{U}_1$ or $\mathbf{U}_2$ with their corresponding linear shear currents — $\mathbf{U}_{1_S}$ and $\mathbf{U}_{2_S}$, respectively — with the same surface vorticity as the corresponding nonlinear shear current. These linear currents are shown as straight lines in Fig. 4.

Fig. 5 depicts the nondimensional intrinsic frequency $\Sigma_0(K(\gamma))$ and group velocity component $\tilde{c}_{gK}$ with respect to K in the presence of $\mathbf{U}_1$, $\mathbf{U}_{1_S}$, and when there is no shear. Significant difference of the solutions to the dispersion relation is observed in Fig. 5a between the presence of $\mathbf{U}_1$ and $\mathbf{U}_{1_S}$ and between the presence and absence of a shear current. For example, as highlighted with circles in Fig. 5a, the K_0 solutions at both $\Sigma_0 = 1.5$
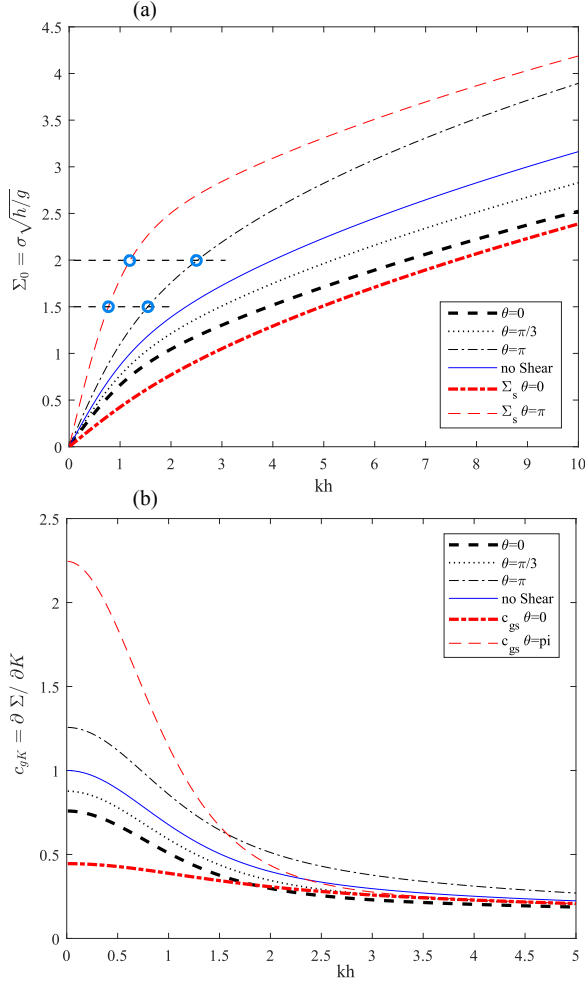
FIGURE 5. Dispersion relation and group velocity with respect to K in the presence of $\mathbf{U}_1$, $\mathbf{U}_{1S}$, and when there is no shear current. In the figure, the parameters $\mathrm{Fr}_h = 0.3$ and $\alpha = 6$ are used; and the subscript s denotes the results in the presence of $\mathbf{U}_{1_S}$.
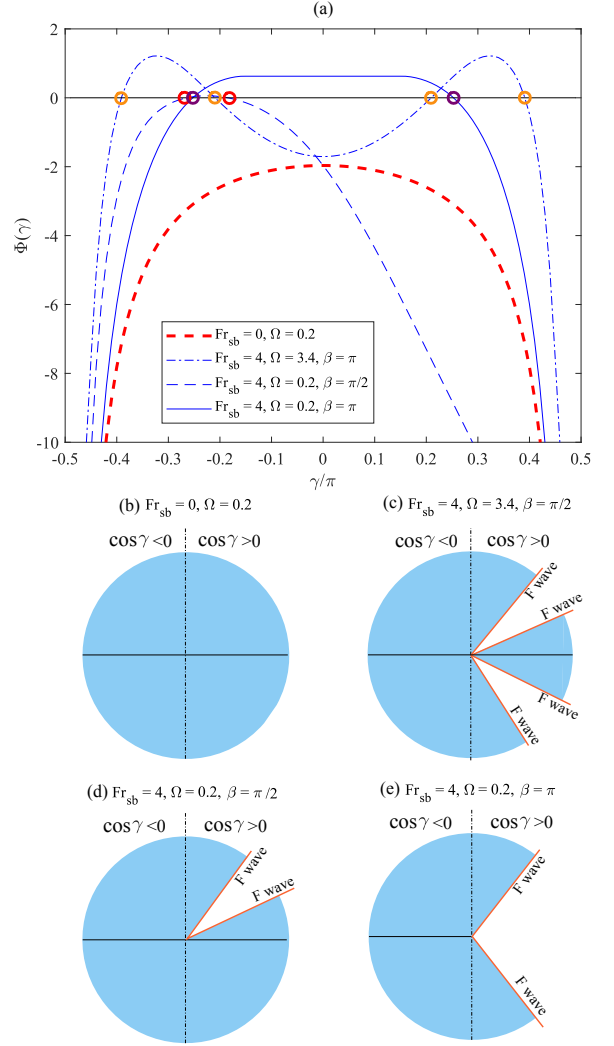

FIGURE 6. Different wave sectors in the absence and presence of a linear shear current. In the figure, $\mathrm{Fr}_h = 0.3$ is used.

and $\Sigma_0 = 2$ in the presence of $\mathbf{U}_{1_S}$ differ by $\approx 100\%$ that for $\mathbf{U}_1$. Moreover, the difference in group velocity among the different cases is even more striking, especially for $0 < K \lesssim 2$, as shown in Fig. 5b.

Based on (16), we plot Φ with respect to $\gamma \in \langle -\pi/2, \pi/2 \rangle$ for different values of the parameters Ω, Fr_{sb}, Fr_h, and β when a linear shear current is present in finite water depth. This is shown in Fig. 6a. For γ values where $\Phi > 0$, no far-field waves exist, as we showed in Sec. 2.3; Fig.6b–e show the excluded sectors corresponding to the parameters of the Φ-graphs in panel a. Panels c, d and e show excluded propagation sectors with no far–field waves. The F waves along different γ_F are marked with circles in Fig.6a, at angles bounding the exclusion sectors. In particular, the γ_F may satisfy (17) that further yields the Doppler resonant value τ_{res}. Note that in the absence of shear, there can only

be one excluded region, symmetrical about $\gamma = 0$, existing when $\tau > 1/4$. A Doppler resonance occurs at values of τ at which one or more exclusion sector appears or disappears. See further discussions in [17].

We now proceed with Doppler resonant frequencies τ_{res} with respect to Fr_h in the presence of $\mathbf{U}_1$, $\mathbf{U}_{1S}$, and when there is no shear, as depicted in Fig. 7. Several interesting phenomena can be observed in the figure. τ_{res} differs in the presence of a shear current from no shear current and depends significantly on the direction of motion of the source relative to the current, β. Moreover, the difference in τ_{res} between the presence of $\mathbf{U}_1$ and $\mathbf{U}_{1S}$ increases with Fr_h in the plotted Fr_h region and may be ignored for $\mathrm{Fr}_h \lesssim 0.08$. This observation can be inferred also from Figs. 3 and 5 where a larger Fr_h tends to yield a relatively smaller Ω_c that corresponds to the F waves of smaller wavenumbers. This sug-
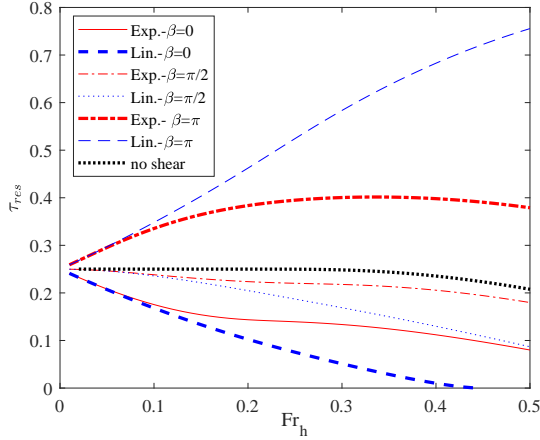
FIGURE 7. Doppler resonant frequencies τ_{res} with respect to Fr_h in the presence of the exponential shear current $\mathbf{U}_1$ (exp.), $\mathbf{U}_{1S}$ (Lin.), and in the absence of a shear current. .

FIGURE 8. Doppler resonant frequencies τ_{res} with respect to Fr_h in the presence of the realistic shear current $\mathbf{U}_2$ (real.), $\mathbf{U}_{2S}$ (Lin.), and in the absence of a shear current.

gests a relatively larger effect of different shear components from a shear current on the group velocity and thus on the Doppler resonance.

Similar phenomena as in Fig.7 are also depicted in Fig.8 where comparisons of τ_{res} among $\mathbf{U}_2$, $\mathbf{U}_{2S}$, and no shear are presented. To our knowledge this is the first time the Doppler resonance for a real, measured oceanographic shear current has been calculated, or indeed a method for doing so has been developed.

Figs. 7 and 8 thus indicate several essential points. Approximating a measured shear current by a linear profile using the surface velocity and shear rate (as is tempting, given that these parameters are readily measured using, e.g. radar techniques [28]), may result in serious errors in the calculated Doppler resonance frequency compared to when the full depth–dependent flow is taken into account. Whether the current be linear or more general of profile, all wave effects are seen to depend strongly on the angle between shear current and direction of motion.

CONCLUSIONS

We have analyzed surface linear waves generated by a moving, oscillating wavemaker in the presence of a horizontal background flow with arbitrary depth–dependence. The necessary theory for finding the resonant oscillation frequency τ_{res} in the presence of such a current is derived, and a direct integration method from [20, 21] is used to obtain numerical results. To our knowledge this is the first time the Doppler resonance frequency has been calculated for a real, measured oceanographic shear current, and indeed that the method for doing so has been presented.

Since it is relatively simple to measure the velocity and vorticity of a shear flow at the free surface, a tempting approxima-
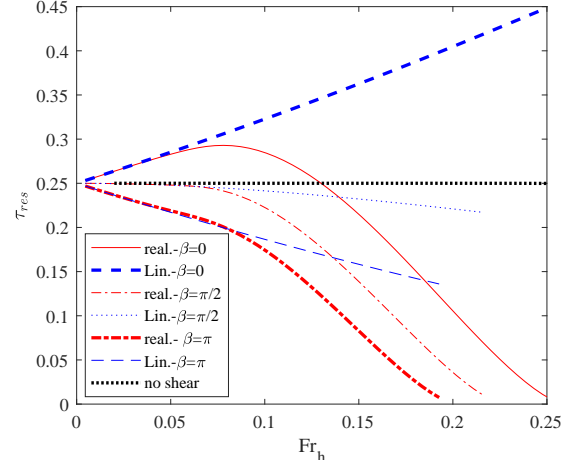
tion is to use a linear shear profile using the surface shear. We show for two different examples of real shear flows that the value of τ_{res} taking the full current profile into account differs substantially from those found assuming no shear or a linear current.

In the presence of a shear current in finite water depth, different far–field waves exist that depend on parameters with respect to the shear current, oscillating frequency and moving speed of the wavemaker, water depth, and the angle between the shear current and the motion of the wavemaker. In particular, two, three or four waves may exist.

The results in the present work suggest that it may be insufficient to model a realistic shear current with a linear shear current of the same surface vorticity, even though the surface vorticity is strong. Full information of a real shear current varying with water depth is of particular practical significance, especially to long and moderate surface waves. It is also demonstrated how, given flow measurements, the Doppler resonant frequency can be readily calculated.

REFERENCES

[1] Haskind, M., 1946. "The hydrodynamic theory of ship oscillations in rolling and pitching". *Prikl. Mat. Mekh, 10*, pp. 33–66.

[2] Brard, R., 1948. "Introduction à l'étude théorique du tangage en marche". *Bulletin de l'ATMA*(47), pp. 455–479.

[3] Wehausen, J. V., and Laitone, E. V., 1960. *Surface waves*. Springer.

[4] Lighthill, M., 1970. "On waves generated in dispersive systems to travelling forcing effects, with applications to the dynamics of rotating fluids". In *Hyperbolic Equations and Waves*. Springer, pp. 124–152.

[5] Dagan, G., and Miloh, T., 1980. "Flow past oscillating bodies at

resonant frequency". In Proc. 13th Symp. on Naval Hydrodynamics, pp. 355–73.

[6] Dagan, G., and Miloh, T., 1982. "Free-surface flow past oscillating singularities at resonant frequency". *Journal of Fluid Mechanics,* *120*, pp. 139–154.

[7] Becker, E., 1956. "Die pulsierende quelle unter der freien oberfläche eines stromes endlicher tiefe". *Ingeniör-Archiv,* *24*(2), pp. 69–76.

[8] Smeltzer, B. K., Li, Y., and Ellingsen, S. Å., 2017. "Effect on doppler resonance from a near-surface shear layer". In ASME 2017 36th International Conference on Ocean, Offshore and Arctic Engineering, American Society of Mechanical Engineers, pp. V07BT06A047–V07BT06A047.

[9] Maruo, H., and Matsunaga, K., 1983. "The slender body approximation in radiation and diffraction problems of a ship with forward speed". In Proc. 12th Scientific and Methodological Seminar on Ship Hydrodynamics (SMSSH).

[10] Kring, D. C., 1998. "Ship seakeeping through the $\tau = 1/4$ critical frequency". *J. Ship Res.,* *42*, pp. 113–119.

[11] Grue, J., and Palm, E., 1985. "Wave radiation and wave diffraction from a submerged body in a uniform current". *Journal of Fluid Mechanics,* *151*, pp. 257–278.

[12] Liu, Y., and Yue, D. K., 1993. "On the solution near the critical frequency for an oscillating and translating body in or near a free surface". *Journal of Fluid Mechanics,* *254*, pp. 251–266.

[13] Ellingsen, S. Å., 2014. "Ship waves in the presence of uniform vorticity". *Journal of Fluid Mechanics,* *742*, p. R2.

[14] Li, Y., and Ellingsen, S. Å., 2016. "Ship waves on uniform shear current at finite depth: wave resistance and critical velocity". *Journal of Fluid Mechanics,* *791*, pp. 539–567.

[15] Li, Y., Smeltzer, B. K., and Ellingsen, S. Å., 2017. "Transient wave resistance upon a real shear current". *European Journal of Mechanics-B/Fluids.* (in press, available online), doi: 10.1016/j.euromechu.2017.08.012.

[16] Li, Y., 2018. "Wave-interference effects on far-field ship waves in the presence of a shear current". *Journal of Ship Research,* *62*(1), pp. 37–47.

[17] Li, Y., and Ellingsen, S. Å., 2016. "Multiple resonances of a moving, oscillating surface disturbance on a shear current". *Journal of Fluid Mechanics,* *808*, pp. 668–689.

[18] Peregrine, D. H., 1976. "Interaction of water waves and currents". *Adv. Appl. Mech.,* *16*, pp. 9–117.

[19] Jonsson, I. G., 1990. "Wave-current interactions". *The sea,* *9*(Part A), pp. 65–120.

[20] Li, Y., 2017. "Surface water waves on depth dependent flows". PhD thesis, Norwegian University of Science and Technology.

[21] Li, Y., and Ellingsen, S. Å., 2017. "Direct integration method for surface waves interacting with a depth dependent flow". (in preparation).

[22] Shrira, V. I., 1993. "Surface waves on shear currents: solution of the boundary-value problem". *Journal of Fluid Mechanics,* *252*, pp. 565–584.

[23] Ellingsen, S. Å., and Li, Y., 2017. "Approximate dispersion relations for waves on arbitrary shear flows". *Journal of Geophysical Research: Oceans,* *122*, pp. 9889–9905.

[24] Dong, Z., and Kirby, J. T., 2012. "Theoretical and numerical study of wave-current interaction in strongly-sheared flows". *Coastal Engineering Proceedings,* *1*(33), p. 2.

[25] Mei, C. C., Stiassnie, M., and Yue, D. K.-P., 2005. Theory and applications of ocean surface waves. part 1: Linear aspects. advanced series on ocean engineering 23.

[26] Chen, X., and Noblesse, F., 1997. "Dispersion relation and far-field waves". In Proceedings of the 12th International Workshop on Water Waves and Floating Bodies, Carry-Le-Rouet, France, pp. 31–35.

[27] Kilcher, L. F., and Nash, J. D., 2010. "Structure and dynamics of the columbia river tidal plume front". *Journal of Geophysical Research: Oceans,* *115*(C5).

[28] Lund, B., Graber, H. C., Tamura, H., Collins, C., and Varlamov, S., 2015. "A new technique for the retrieval of near-surface vertical current shear from marine x-band radar images". *Journal of Geophysical Research: Oceans,* *120*(12), pp. 8466–8486.